Flexural performance of reinforced concrete beams strengthened with prestressed near-surface-mounted FRP reinforcements

by

Ilker Fatih Kara[a,b,*], Ashraf F. Ashour[b] and Mehmet Alpaslan Köroğlu[b,c]

[a]Civil Engineering Department, Nigde University, Nigde, Turkey

[b]School of Engineering, University of Bradford, BD7 1DP, UK

[c]Civil Engineering Department, Necmettin Erbakan University, Konya, Turkey

Abstract

A numerical method for estimating the curvature, deflection and moment capacity of reinforced concrete beams strengthened with prestressed near-surface-mounted (NSM) FRP bars/strips is presented. A sectional analysis is carried out to predict the moment-curvature relationship from which beam deflections and moment capacity are then calculated. Based on the amount of FRP bars, different failure modes were identified, namely tensile rupture of prestressed FRP bars and concrete crushing before or after yielding of steel reinforcement. Comparisons between experimental results available in the literature and predicted curvature, moment capacity and deflection of reinforced concrete beams with prestressed NSM FRP reinforcements show good agreement. A parametric study concluded that higher prestressing levels improved the cracking and yielding loads, but decreased the beam ductility compared with beams strengthened with nonprestressed NSM FRP bars/strips.

Keywords: A: Fibres; A:Hybrid; B: Corrosion; C: Numerical Analysis

1. Introduction

Fibre reinforced polymer (FRP) strengthening techniques in form of externally bonded (EB) or near-surface mounted (NSM) have recently become one of the most effective upgrading method for reinforced concrete (RC) members [1]. However, the brittle debonding or peeling failure of EB FRP reinforcements from strengthened members, especially in zones of high flexural and shear stresses limits the efficiency of EB strengthening method as it prevents the

strengthened members from achieving their maximum flexural/shear load capacities [2]. EB FRP reinforcements could also be highly susceptible to damage from collision, fire, ultraviolet rays, and moisture absorption [3]. To minimize these problems, and to improve the utilization of FRP materials, near-surface mounted reinforcement was recently introduced as a promising technique for strengthening reinforced concrete members [4-6]. NSM FRP reinforcement has better bonding to concrete than EB FRP systems and is also protected from natural hazards by concrete cover and less exposed to accidental damages [5].

Although flexural strengthening using NSM FRP reinforcement can remarkably increase the ultimate strength of RC members, their contribution to member stiffness and deflections is limited owing to the low FRP modulus of elasticity. Therefore, prestressed NSM FRP reinforcement has been recently implemented in reinforced concrete elements [7-9] to improve the efficiency of NSM strengthening technique. Prestressing NSM FRP reinforcement decreases stresses in both concrete and steel reinforcement as well as member deflections. However, the ductility of the prestressed strengthened beam is reduced compared with a non-prestressed strengthened beam as a portion of strain capacity of FRP reinforcement has already been used in prestressing.

In the published literature, numerous research investigations (listed in [6]) have been reported on the flexural behaviour of RC members strengthened with non-prestressed NSM FRP reinforcement, but limited studies have been recently conducted on the use of prestressed NSM FRP reinforcement for strengthening RC structures [7-23]. Nordin and Täljsten [10] tested fifteen full-scale RC beams under static loadings with various combinations of prestressed NSM FRP. They concluded that concrete cracking and steel yielding load of the prestressed NSM FRP strengthened beams were increased and crack width was reduced compared with nonprestressed NSM FRP beams, leading to better durability. They also noted that the losses of stresses in NSM FRP reinforcement ranged from 2.8 -14.5% at the bar centre and 35-100% at the bar ends. The study by Badawi and Soudki [11-13] on reinforced concrete beams strengthened with prestressed NSM FRP rods under monotonic and fatigue loadings highlighted the enhancement of flexural performance of beams strengthened with prestressed NSM FRP. In other investigations, Oudah and El-Hacha [8, 14] found that increasing the prestressing levels of CFRP strips improved the service conditions but reduced the ductility of the beams tested. They also concluded that the fatigue life of the beams tested has been enhanced by reducing strains in steel reinforcement.

In the present study, a numerical method has been developed for the prediction of the moment–curvature relationship and, hence, moment capacity and deflections of reinforced concrete beams strengthened with prestressed NSM FRP rods. The validity of the proposed numerical model has been assessed by simulating the behaviour of experimentally tested RC beams strengthened with prestressed or non-prestressed NSM CFRP reinforcements. The effect of prestressing level on cracking, yielding, and ultimate loads were also investigated. The present study has also evaluated the applicability of various equations available in the literature for deflection predictions of FRP RC beams to RC beams strengthened with prestressed FRP rods.

2. Numerical approach

A numerical method for estimating the curvature, deflection and moment capacity of reinforced concrete beams strengthened with prestressed NSM FRP rods is developed. Force equilibrium and strain compatibility equations for a beam section divided into a number of segments are numerically solved due to the non-linear behaviour of concrete. The deflection is then obtained from the flexural rigidity at the mid-span section using the deflection formula for various load cases. The following section describes the process in greater details.

2.1 Constitutive laws of the materials

The stress-strain relationships of concrete, steel and prestressed FRP reinforcements implemented in this investigation are shown in Figure 1. However, the numerical technique proposed can accommodate other material models. CEB-FIP [24] model is adopted for concrete stress-strain relationship in compression as shown in Figure 1(a). This model can be represented by the following equations:

$$f_c = f_c^{'}\left(\frac{2\varepsilon_c}{\varepsilon_{co}} - \left(\frac{\varepsilon_c}{\varepsilon_{co}}\right)^2\right) \qquad \varepsilon_c < \varepsilon_{co} \qquad (1(a))$$

$$f_c = f_c^{'} \qquad \varepsilon_{co} \le \varepsilon_c \le \varepsilon_{cu} \qquad (1(b))$$

where f_c and ε_c are the compressive stress and strain in concrete, respectively, $f_c^{'}$ is the cylinder compressive strength of concrete, ε_{co} (=0.002) is the strain in concrete at maximum stress and ε_{cu} (=0.0035) is the ultimate strain of concrete as shown in Figure 1(a).

A bi-linear stress-strain relationship is adopted to model concrete in tension as shown in Figure 1(b) and given below:

$$f_t = E_t \varepsilon_t \qquad \varepsilon_t \le \varepsilon_{ct} \qquad \text{((2(a))}$$

$$f_t = f_{tu} - \frac{f_{tu}}{\mu \varepsilon_{ct}} \left(\varepsilon_t - \varepsilon_{ct} \right) \qquad \varepsilon_{ct}(1+\mu) \ge \varepsilon_t > \varepsilon_{ct} \qquad \text{((2(b))}$$

where f_t and ε_t are the tensile stress and strain in concrete, respectively, f_{tu} $(=0.62\sqrt{f_c'})$ and ε_{ct} are the tensile strength and corresponding tensile strain of concrete, respectively, E_t is the tensile modulus of concrete, assumed to be the same as E_c, and μ is a factor controlling the rate of tensile strength decay.

Reinforcing steel is modelled as an elastic-plastic material with yield stress f_y as shown in Figure 1(c). The stress-strain relationship of FRP reinforcement is linear elastic up to rupture and given by:

$$f_f = E_f \varepsilon_{frpt} \qquad \varepsilon_{frpt} \le \varepsilon_{fu} \qquad (3)$$

where f_f and E_f are the stress and modulus of elasticity of FRP bars, ε_{frpt} is the strain in FRP bars, and f_{fu} and ε_{fu} are the ultimate strength and strain of FRP bars, respectively, as shown in Figure 1(d). The total strain ε_{frpt} in FRP reinforcement consists of the following strain values at different loading stages,

$$\varepsilon_{frpt} = \varepsilon_{frp(press)} + \varepsilon_{frp(c)} + \varepsilon_{frp(load)} \qquad (4)$$

in which $\varepsilon_{frp(pres)}$ is the strain in FRP reinforcements due to the initial prestressing force, $\varepsilon_{frp(c)}$ is the strain in FRP at decompression in concrete at level of bars and $\varepsilon_{frp(load)}$ is the strain in FRP due to external applied loads.

2.2 Moment–curvature relationship of FRP reinforced concrete sections

The moment–curvature (M–φ) relationship of RC beams strengthened with prestressed FRP reinforcement can be idealized by three different zones as depicted in Fig. 2. The first region signifies the pre-cracking stage of concrete between the initial camber (point (ci)) and initiation of concrete cracks (point (ccr)), the intermediate zone represents the post-cracking

to steel yield initiation (point (sy)), followed by the post-yielding stage to the ultimate capacity point (uc). The strain distribution across the beam section at each of these points is also schematically shown in Fig. 2.

It is to be noted that the effect of any sustained loads (for example dead loads) acting on the beam before the application of the prestressing force is not taken into account in the present loading sequence presented in Fig. 2. Such load effects would cause tensile strains and stresses in the longitudinal steel reinforcement and surrounding concrete and, consequently, the release of the prestressing force should reduce the tensile stresses induced by these loads.

When releasing the prestressing force, an initial compression field in the longitudinal steel bars and surrounding concrete is introduced [10, 25, 26]. As the external loads increase, these compressive strains are converted to tensile strains. As expected, the load carrying capacities corresponding to concrete cracking and steel yielding initiation increase with the increase in the level of prestressing due to its initial compressive strain profile.

Figure 3 shows the strain distributions of a concrete section reinforced with top and bottom steel reinforcing bars as well as prestressed FRP reinforcement due to initial prestressing. When FRP reinforcement is applied with a certain prestressing level, an initial negative camber (upward deflection) is exhibited due to the eccentricity (e) of the prestressing force (T_{pr}) in relation to the centroidal axis of the cross section (Fig. 3) at the pre-cracking stage. This negative camber causes a tensile strain at the top fibre (ε_{cpti}) and a compressive strain at the bottom fibre (ε_{cpbi}) of concrete. The equations of centroidal axis depth, c_{pi}, transformed un-cracked second moment I_{uncr} of area, tensile and compressive strains at the top and bottom fibres are given below for the pre-cracking initial negative camber stage:

$$c_{pi} = \frac{b\,h^2/2 + A_s'(n_s-1)d_s' + A_s(n_s-1)d_s + A_f n_f d_f - A_{grv} d_f}{bh + A_s'(n_s-1) + A_s(n_s-1) + A_f n_f - A_{grv}} \tag{5}$$

$$I_{uncr} = \frac{bh^3}{12} + bh\,(c_{pi} - \frac{h}{2})^2 + A_s'(n_s-1)\,(c_{pi} - d_s')^2 + A_s(n_s-1)\,(c_{pi} - d_s)^2 + A_f n_f\,(c_{pi} - d_f)^2 - A_{grv}(d_f - c_{pi})^2 \tag{6}$$

$$\varepsilon_{\text{cpti}} = \frac{T_{pr} e\, c_{pi}}{E_c I_{uncr}} - \frac{T_{pr}}{E_c bh} \tag{7}$$

$$\varepsilon_{\text{cpbi}} = \frac{T_{pr} e\,(h - c_{pi})}{E_c I_{uncr}} + \frac{T_{pr}}{E_c bh} \tag{8}$$

where A_{grv} is the area of prestressed NSM FRP reinforcement groove; A_s and $A_s^{'}$ are the area of bottom and top steel reinforcing bars, respectively, A_f is the area of prestressed NSM FRP bars, n_s and n_f are the modular ratio of steel and FRP reinforcement to concrete, respectively, h is the beam depth and b is the beam width, d_f is the bottom FRP reinforcement depths, d_s and $d_s^{'}$ are the bottom and top steel reinforcement depths, respectively. In fact, due to the short-term prestress losses in FRP reinforcement after the release of the prestressing force, the effective prestressing force should be used in Eqs. (7) and (8) instead of the applied prestressing force (T_{pr}). However, the effect of these short-term prestrain losses was neglected in order to simplify the calculation procedure. It was also reported [10] that these initial losses are very small. It should be also noted that Eq. (7) are derived by assuming that no cracking occurs after the release of the prestressing force.

The initial negative curvature of the prestressed strengthened beams (φ_i) can be determined by considering the neutral axis depth from the extreme top fibre of concrete (x_{pi}) as follows:

$$x_{\mathrm{pi}} = \frac{\varepsilon_{cpti}\, h}{(\varepsilon_{cpti} + \varepsilon_{cpbi})} \tag{9}$$

$$\varphi_{\mathrm{i}} = \frac{\varepsilon_{cpti}}{x_{\mathrm{pi}}} \tag{10}$$

As the external lateral loads increase, the compressive strains in the bottom fiber concrete are changed to tensile strains, followed by concrete cracking, initiation of steel yielding and post yielding stages up to ultimate flexural failure as shown in Fig 2.

Figure 4 presents a reinforced concrete section strengthened with prestressed FRP after releasing the prestressing force and applying the actual working loads. The beam cross section is divided into a number of segments, n, to accommodate the nonlinear stress-strain relationships of concrete and steel in the analysis. The iterative numerical procedure starts by assuming a small value of strain at the concrete extreme compression fibre. For each strain ε_c at the top level of concrete section, the neutral axis depth, x, is initially assumed and the correct value is iteratively obtained when equilibrium of forces is satisfied. According to the assumption that plane section before bending remains plane after bending, the strain in each concrete segment is linearly proportional to its distance from the neutral axis (Figure 4) as expressed below:

$$\varepsilon_i = \frac{x - x_i}{x}\varepsilon_c \tag{11}$$

where ε_c is the strain at the top compression level of the reinforced concrete section and ε_i is the concrete compressive or tensile strain at mid-depth of *i*-th segment.

Assuming perfect bond between concrete and reinforcing bars and strain compatibility, strains in tensile and compressive reinforcing steel and prestressed FRP bars can also be obtained from:

$$\varepsilon_{frp(load)} = \frac{x - d_f}{x}\varepsilon_c \tag{12}$$

$$\varepsilon_s = \frac{x - d_s}{x}\varepsilon_c \tag{13}$$

$$\varepsilon_s^{'} = \frac{x - d_s^{'}}{x}\varepsilon_c \tag{14}$$

where $\varepsilon_{frp(load)}$ indicates the strains in bottom prestressed FRP bars due to loading, ε_S and $\varepsilon_S^{'}$ are the strain in bottom and top reinforcing steel bars, respectively.

The corresponding stresses in each concrete segment, and tensile and compressive steel and FRP reinforcements can be calculated from the respective stress-strain relationships of concrete and reinforcements presented in Figure 1. The total concrete force including the contribution of compressive and tensile forces is calculated using Eq. (15) below:

$$F_c = \sum_{i=1}^{n} f_{ci} h_i b \tag{15}$$

where f_{ci} is the concrete compressive or tensile stress at the centroid of the *i*-th segment, h_i (=*h*/*n*) is the thickness of the *i*-th segment, *n* is the total number of section segments. This summation extends over all compressive and tensile concrete segments. The forces in bottom and top reinforcing bars are estimated from:

$$T_f = A_f E_f (\varepsilon_{frp(press)} + \varepsilon_{fpr(c)} + \varepsilon_{fpr(load)}) \quad \text{and} \quad T_S = A_S E_S \varepsilon_S \tag{16}$$

$$C_S = A_S^{'} E_S^{'} \varepsilon_S^{'} \tag{17}$$

T_f and E_f are the force and modulus of elasticity of bottom reinforcing prestressed FRP bars, respectively. In the same equations, T_s and E_s are the force and modulus of elasticity of bottom reinforcing steel bars, and C_s and $E_S^{'}$ are the corresponding values of top steel reinforcement. Eqs. (16) and (17) are also valid for different types of FRP bars, i.e., GFRP, AFRP and CFRP, provided that the appropriate modulus of elasticity, E_f, and tensile rupture, f_{fu}, are used. Considering equilibrium of forces, the following equation is obtained:

$$F_c + C_s = T_f + T_s \tag{18a}$$

$$\sum_{i=1}^{n} f_{ci} h_i b + A_s^{'} E_s^{'} \varepsilon_s^{'} = A_f E_f (\varepsilon_{frp(press)} + \varepsilon_{fpr(c)} + \varepsilon_{fpr(load)}) + A_s E_s \varepsilon_s \tag{18b}$$

In the above Eqs. (18), the neutral axis depth x is the only unknown. The value of x is iteratively adjusted using the bi-section method until sufficient equilibrium accuracy is attained, for example:

$$\frac{\left| F_c + C_s - T_f - T_s \right|}{\left| F_c \right|} \leq 10^{-8} \tag{19}$$

The beam curvature φ can also be determined from the strain distribution as follows (see Figure 4(b)):

$$\varphi = \frac{\varepsilon_c}{x} \tag{20}$$

The applied moment M_f of the section is then calculated by taking moments of internal forces about any horizontal axis, for instance about the neutral axis:

$$M_f = \sum_{i=1}^{n} F_{ci} (x - x_i) + T_f (x - d_f) + T_s (x - d_s) + C_s (x - d_s') \tag{21}$$

where F_{ci} ($=f_{ci}h_ib$) is the concrete compressive or tensile force at the centroid of the i-th segment.

The strain in the extreme concrete compression fibre is incrementally increased and the above procedure is repeated for each value of strain until the maximum concrete compressive strain reaches its ultimate compressive strain (ε_{cu} =0.0035). During such strain increase, concrete crushing, rupture of FRP bars or yielding of steel reinforcement may occur depending on the amount of steel and prestressed FRP reinforcement provided. The section moment capacity M_{fu} is, therefore, the highest moment attained for various increments considered until failure. Based on the aforementioned procedure, a computer program has been developed for the moment-curvature relationship and moment capacity of reinforced concrete sections strengthened with non-prestressed and prestressed FRP reinforcement. The initial strains and negative curvature of the prestressed strengthened beams are also included in the analysis as presented in Eqs. (7-10).

The present numerical method assumes perfect bond between concrete and reinforcing FRP bars/strips. However, there could be slip occurring between FRP bars and the epoxy (epoxy-concrete interface along FRP bars), possibly due to shear deformation in the epoxy, resulting in strain incompatibility between the rod and surrounding concrete at the level of FRP bars/strips. As such bond slip occurs, the prestress loss could occur and the predicted load-midspan deflection curves could also be stiffer than the experimental curves. Moreover, the strengthened beams may eventually fail due to the debonding of FRP bars, which results in a poor ductility and an inadequate utilization of FRP strength. The analysis considering the interface debonding can be carried out by means of finite element modelling [1, 27] rather than the sectional analysis. The interface slip between concrete and FRP bar/strips can be considered within the element formulation and the bond-slip law could be applied for describing the interaction between concrete and FRP strips.

2.3 Validation of the proposed numerical model

2.3.1. Flexural capacity prediction

Test results of 17 reinforced concrete beams strengthened with FRP bars/strips collected from previous experimental investigations in the literature [7, 9-11, 15, 18] are used to validate the proposed numerical method. Table 1 lists the geometrical and material properties of all beams

considered. The level of the prestressing force applied to FRP reinforcements varied between 20% and 60% of their tensile strength. All the 17 beams were reported to have failed in flexure; either by concrete crushing or FRP rupture failure modes. Comparisons between predictions from the current numerical technique and flexural moment capacities of all beams are presented in Table 2 and Figure 5. The average and standard deviation of the ratio between the present technique and experimental bending capacities, M_{the}/M_{exp}, are 1.08 and 19%, respectively. The ratio of M_{the}/M_{exp} varies between 0.80 and 1.36. Overall, the predictions obtained from the current analysis are in good agreement with the experimental results except for the beam series of BPS1 to BPS5. It is to be noted that the tensile rupture strength of CFRP bars used in BPS1 to BPS5 quoted in the original investigation [10] was exceptionally higher than that of CFRP bars used for the other group BPM1 to BPM4. However, when the tensile strength of CFRP bars in beams BPS1 to BPS5 is assumed to be the same as that for beams BPM1 to BPM4 of the same investigation, the predictions from the current technique are far much improved as presented in Table 2. The failure modes are also correctly predicted by the present technique for 16 beams considered as reported in Table 2.

2.3.2. Moment–curvature relationship

The moment–curvature results obtained from the numerical technique are compared with the experimental results of reinforced concrete beams strengthened with prestressed FRP strips tested by El-Hacha and Gaafar [9] as shown in Fig. 6. The geometrical dimensions, reinforcement details and material properties of reinforced concrete beams considered are given in Table 1.

The numerical results obtained from the present technique are in good agreement with the test results beams as depicted in Figure 6. It also indicates that the proposed technique is able to accurately predict various features of the moment-curvature relationship, including the first cracking load, yielding and post yielding of steel, and eventually FRP rupture.

3. Effect of prestressing force and amount of FRP reinforcement

The proposed numerical technique has been employed to study the effect of prestressing level and amount of FRP reinforcement on the moment-curvature relationship as presented below.

3.1 Effect of amount of FRP reinforcement

The influence of the amount of FRP bars/strips was examined by comparing the moment curvature relationships of reinforced concrete beams as predicted in Fig. 7: Fig. 7a for under reinforced and Fig. 7b for over reinforced sections.

The dimensions and concrete properties are the same for all beams considered in Figure 7; *b = 200 mm, h = 300 mm,* $f_c' = 35\ N/mm^2$, $E_f=160\ kN/mm^2$, $f_{fu}=2800\ N/mm^2$, $f_{(pr)}(T_{pr}/A_f)=560\ N/mm^2$, $A_s=402\ mm^2$ and $f_y=480\ N/mm^2$. It can be observed from Figure 7 (a-b) that the initial linear stiffness is similar for all beams studied. The end of the linear phase is identified by concrete cracking and, consequently, reinforcing bars play a more significant role in controlling the beam stiffness depending on the amount of FRP reinforcement. After cracking, the moment-curvature relationship has a less gradient than the initial uncracked part owing to the decrease in the beam stiffness. The reduction in stiffness due to cracking is almost the same in the beams having different amount of FRP reinforcement for both under and over reinforced case. The end of the second part of moment curvature relationships marked the yielding of tensile steel reinforcement, and was followed by a softer slope until FRP rupture or concrete crushing. In this phase, FRP prestressed reinforcement showed a more influential role in resisting loads after yielding of steel. As seen in Figure 7(a-b), the beam stiffness increases with the increase of prestressed FRP reinforcement after the steel yielding; the higher the amount of presetressed NSM FRP reinforcement, the higher the stiffness. For the underreinforced concrete section, although there is a sudden drop in bending moment resulted from the rupture of FRP bars, some residual ductility is exhibited by the beam up to concrete crushing as the steel reinforcement is still far below its breaking point (Figure 7(a)). The results show that the concrete cracking and steel yielding loads increase with the incerase in the area of FRP reinforcement for both under reinforced and over reinforced sections.

3.2 Effect of prestressing level

The current numerical technique has also been employed to study the effect of prestressing level on the flexural behavior of strengthened RC beams as depicted in Figure 8. The dimensions, concrete properties, amount of steel and FRP reinforcement and loading of beams in Fig. 8 are similar to the beams tested by Badawi and Soudki [10]*; b = 152 mm, h = 254 mm,* $f_c = 35N/mm^2$, $A_f=70.85\ mm^2$, $A_s=402\ mm^2$, $f_y=480\ N/mm^2$; $f_{fu}=1970\ N/mm^2$ *and* $E_f=136\ kN/mm^2$. The level of the prestressing force for FRP reinforcement changed between 20% and 80% of tensile strength of FRP reinforcement used in the beams. Figure 8 indicates that all the

strengthened beams exhibit similar behaviour before or after concrete cracking and steel yielding.

The effect of increasing the prestressing level on the cracking, yielding, and ultimate moments of the same beams is shown in Figure 9. It can be observed that increasing the prestressing levels significantly increased the cracking loads but had almost no effect on the ultimate loads as also concluded in [9, 10]. The forces that were introduced in the lower part of the beam due to FRP prestressing increased the loads needed to create cracks in concrete. As higher prestressing forces lead to higher stresses in concrete and steel, higher loads are needed to counteract those forces. As for the steel yielding, the higher prestressing levels delay the steel yielding to higher loads.

Figure 10 shows the effect of the prestressing level on the ductility index of the beams considered above. The ductility index is taken as the ratio of the deflection at the ultimate load to that at a load causing yielding in the tension steel reinforcement. The ductility of the unstrengthened beam, shown for comparison purposes, is also calculated. As seen in Fig. 10, the ductility index continuously decreases as the prestressing level increases. For a range of prestressing between 0% and 60% considered in this study, there is a roughly linear relationship between the reduction of the ductility index of the strengthened beams and the prestressing level especially after the 20% prestress level. The reductions in the ductility index compared to the control beam for the 0%, 20%, 40% and 60% prestressed strengthened beams are 43%, 47%, 60%, and 72%. It should be expressed that the beams with a higher prestressing level lost part of their ductility at failure due to the fact that a large proportion of the possible strain in the FRP reinforcement was used during prestressing, resulting in failure at a smaller curvature and thus deflections.

Fig. 11 also indicates the variation of flexural rigidity, EI_{eff}, of beams with different prestressing level against the applied moment. The effective flexural rigidity curve consists of different segments, indicating the pre-cracking, post-cracking, yielding of steel, and FRP rupture. In the pre-cracking stage, the beams showed the highest flexural stiffness. Once the beams cracked, the flexural rigidity was notably reduced but remained almost constant until yielding of steel reinforcement. A further reduction of EI_{eff} is depicted after the yielding of tensile steel reinforcement up to FRP rupture. Fig. 11 indicates that all the beams with different prestressing levels follow nearly the same trend except for beams with 80% of prestressing levels reaching its FRP rupture stage before steel yielding.

4. Failure modes of reinforced concrete beams strengthened with FRP bars/strips

The balanced condition for reinforced concrete beams reinforced with prestressed NSM FRP bars is proposed in a way such that concrete crushing in compression and rupture of FRP reinforcement simultaneously occur, while steel reinforcement would have already yielded [26]. According to the existing research, the most common failure mode of the prestressed NSM beams was the rupture of FRP reinforcement [7-23]. This failure mode could be attributed to the relatively low FRP section area-to-beam width ratio as each beam was typically strengthened with one FRP reinforcement. However, there will always be the requirement of using multiple FRP reinforcements when the load-carrying capacity of structures needs to be significantly increased. Figure 12 shows the strain distribution for various modes of failure as explained below in more details.

4.1 Mode I: Tensile rupture of prestressed FRP bars

When $\varepsilon_c = \varepsilon_{cu}$ and $\varepsilon_{fprt} = \varepsilon_{fu}$ simultaneously take place, the strain distribution is unique and the neutral axis depth x_l is calculated using Eq. (12) with $\varepsilon_{frp(load)}$ and ε_c replaced by ε_{fu} and 0.0035, respectively:

$$x_l = d_f \frac{0.0035}{0.0035 + \varepsilon_{fu}} \tag{22}$$

When the area A_f of FRP reinforcement is below a certain value A_{fl}, FRP brittle rupture occurs before concrete crushing. For a given area A_s of steel reinforcement, the limiting area A_{fl} of FRP bars can be readily calculated from Eq. 18(b) with f_s and f_f replaced by f_y and f_{fu}, respectively:

$$A_{fl} = \frac{\sum_{i=1}^{n} f_{ci} b h_i + A'_s E'_S \varepsilon'_S - A_s f_y}{f_u} \tag{23}$$

where ε'_s is calculated from Eq. (14) with x and ε_c replaced by x_l and *0·0035*, respectively. The area A_{fl} of FRP bars (given by Eq. (23)) forms a lower limit for the amount of FRP bars in order to avoid tensile FRP rupture. Figure 12(a) shows the strain distribution in case of $A_f < A_{fl}$.

4.2 Mode II: Yielding of steel reinforcement followed by crushing of concrete

This mode of failure is characterized by yielding of steel reinforcement followed by crushing of concrete, before rupture of FRP reinforcement (see Figure 12(b) for strain distribution). In this case, the area of prestressed NSM FRP bars exceeds A_{fl}, therefore tensile rupture of prestressed NSM FRP bars would not occur. This case is similar to the under-reinforced section of conventional reinforced concrete beams. The upper limit to the area of FRP bars, A_{fu}, is attained when strains ε_c in the extreme compression fibre of concrete and ε_s in the tension reinforcement simultaneously reach ε_{cu} and ε_y, respectively. By following similar calculations to those presented above for mode I, the neutral axis depth x_u and the area A_{fu} of FRP bars corresponding to this upper limit of FRP bars are calculated from:

$$x_u = d_s \frac{0.0035}{0.0035 + \varepsilon_y} \tag{24}$$

$$A_{fu} = \frac{\sum_{i=1}^{n} f_{ci} b h_i + A'_s E'_S \varepsilon'_S - A_s f_y}{E_f(\varepsilon_{frpt})} \tag{25}$$

where ε'_s and ε_{frpt} are calculated from Eqs. (4), (12) and (14), with x and ε_c replaced by x_u and *0·0035*, respectively.

The neutral axis depth x_u given by Eq. (24) is the same as that defining the balanced section for conventional reinforced concrete beams. To ensure ductile flexural behaviour, the area of FRP bars provided should be smaller than A_{fu} given in Eq. (25) and greater than A_{fl} to achieve ductile failure by yielding of steel reinforcement and crushing of concrete, before rupture of FRP reinforcement.

4.3 Mode III: Crushing of concrete before yielding of steel reinforcement (over-reinforced case)

If the area of FRP bars used exceeds A_{fu}, the concrete strain ε_c reaches the ultimate value ε_{cu} before any yielding of tension reinforcement or FRP rupture as shown in Figure 12(c). In this case, there is a large amount of steel and FRP bars and the section is over-reinforced. Such

failure, often explosive, occurs with little warning, similar to that of conventional over reinforced concrete beams.

4.4 Effect of size of steel and prestressed FRP bars/strips on the bending capacity

Figure 13 presents the effect of steel and prestressed FRP reinforcements on the normalized moment capacity η (= M_f/bd^2): Figure 13(a) shows the variation of the normalized moment capacity η against the steel reinforcement ratio ρ_s (= $100A_s/bd$) whereas Figure 13(b) gives the variation of the normalized moment capacity η against the FRP reinforcement ratio ρ_f (= $100A_f/bd$). The dotted lines in Figure 13 represent the boundaries of different flexural failure modes as explained above.

The effect of prestressed FRP reinforcement on moment capacity is more pronounced for strengthened reinforced concrete sections having less area of steel reinforcement when mode I and mode II dominate the flexural behaviour of reinforced concrete beams. However, the rate of the effect of FRP reinforcement decreases as the amount of steel reinforcement increases. On the other hand, the increase in the normalized moment capacity η is insignificant when mode III (crushing of concrete before yielding of steel and rupture of FRP) dominates the flexural failure. The higher the amount of prestressed NSM FRP bars, the less the rate of increase of the normalized moment capacity η for the same amount of steel reinforcement ratio ρ_s. Therefore, the upper limit for the area of prestressed NSM FRP reinforcement, A_{fu} given by (Eq. (25)), indicates the optimum use of FRP reinforcement and exhibits more ductility. However, it should be noted that, with the increase of FRP section area-to-beam width ratio, the failure mode may be changed as there is a probability that concrete cover cannot resist the normal and shear stresses induced by NSM FRP reinforcements.

5. Deflection predictions

In this section, a simplified method for deflection calculation of reinforced concrete beams strengthened with prestressed NSM FRP rods is developed from the moment-curvature relationship presented above. The effective flexural rigidity, EI_{eff}, of the member at the location of the maximum moment is firstly determined from the moment–curvature relationship at each loading as:

$$EI_{eff} = \frac{M}{\varphi} \tag{26}$$

The mid-span deflection, Δ, of strengthened reinforced concrete beams is then calculated using the elastic deflection formula, for example, the immediate deflection of simply supported beams loaded with two-point loads, each P/2, could be also computed from Eq. (27) as follows:

$$\Delta = \frac{(P/2)(3L^2 - 4a^2)}{24EI_{eff}} \tag{27}$$

where a is the shear span and L is the beam span length. The initial camber of the strengthened beams due the initial prestressing force, T_{pr}, can also be computed by considering the constant curvature variation due to the prestressed end moment M_{pr} (=T_{pr}*e, where e is the force eccentricity) as:

$$\Delta = \frac{M_{pr}L^2}{8EI_{uncr}} \tag{28}$$

This initial camber has to be allowed for when calculating the total beam deflection. The applicability of different models available in the literature for deflection calculations of FRP reinforced concrete beams to RC concrete beams strengthened with prestressed FRP reinforcement is also evaluated by comparing their predictions against the experimental results as well as the current numerical technique.

The ACI Committee 440-06 [6] provides a modified version of Branson's equation that includes a reduction coefficient, β_d, related to the reduced tension stiffening exhibited by FRP reinforced concrete members as follows:

$$\mathrm{I_{eff}} = \left(\frac{\mathrm{M_{cr}}}{\mathrm{M}}\right)^3 \beta_\mathrm{d}\mathrm{I_1} + \left[1 - \left(\frac{\mathrm{M_{cr}}}{\mathrm{M}}\right)^3\right]\mathrm{I_2} \tag{29}$$

$$\beta_\mathrm{d} = 0.2\left(\frac{\rho_\mathrm{f}}{\rho_\mathrm{fb}}\right) \tag{30}$$

where I_1 and I_2 are the moments of inertia of the gross and cracked transformed concrete sections considering the contribution of steel and FRP reinforcement to the stiffness, respectively, M is the applied bending moment, M_{cr} is the flexural cracking moment, $ß_d$ is a reduction coefficient given by Eq. (30), ρ_f $(=A_f/bd)$ is the FRP reinforcement ratio, A_f is the area of tensile FRP reinforcement, b and d are width and effective depth of FRP reinforced concrete beams and ρ_{fb} is the balanced FRP reinforcement ratio.

ISIS Canadian network design manual [28] suggested that the effective moment I_{eff} of inertia for deflection calculations of FRP reinforced concrete members can be taken as:

$$I_{eff} = \left(\frac{I_1 I_2}{I_1 + \left(1 - 0.5\left(\frac{M_{cr}}{M}\right)^2 (I_1 - I_2)\right)} \right) \tag{31}$$

On the other hand, Bischoff [29] recommended the following expression related to an equivalent moment of inertia based on the tension-stiffening effect on curvature:

$$I_{eff} = \left(\frac{I_2}{1 - \left(1 - \frac{I_2}{I_1}\right)\left(\frac{M_{cr}}{M}\right)^2} \right) \tag{32}$$

The mid-span experimental deflections of beams tested by Gaafar and El-Hacha [9] and Badawi and Soudki [11] are compared with the predictions from the current numerical technique and other models in Eqs. (29) to (32); see Figure 14(a-d). The geometrical dimensions, reinforcement details and material properties of beams considered are given in Table 1. The deflection results obtained from the present numerical technique agree well with the test results. Figure 14 indicates that the present technique is able to predict both the pre and post cracking deflections and to capture the beam stiffness and deflection after yielding of steel. Figure 14 also shows that the deflections predicted by different models compare well at low load levels before and after the first cracking load. However, the predictions of all the models considered significantly underestimate the experimental results for high load levels.

5. Conclusions

An iterative numerical method based on equilibrium of forces and compatibility of strains has been developed to evaluate the moment-curvature relationship, moment capacity and deflections of reinforced concrete beams strengthened with prestressed NSM FRP rods. Comparisons between the predicted moment capacity, curvatures and deflections of strengthened reinforced concrete beams and experimental results available in the literature show good agreement.The proposed method is able to predict both the pre and post cracking deflections up to the beam failure and to capture the beam behaviour after yielding of steel reinforcements. The deflections predicted by different models compare well at low load levels before and after the first cracking load, but, for high load levels, the predictions of all models considered significantly underestimate the experimental results.

A parametric study concluded that the use of prestressed NSM FRP reinforcement in reinforced concrete beams improved the service conditions of beams. Increasing the prestressing levels increased the cracking and yielding loads but had almost no effect on the ultimate loads. The ductility of beams also decreases as the prestressing level increases.

Acknowledgment

The authors acknowledges the financial support of the Scientific and Technological Research Council of Turkey (TUBİTAK).

References

[1] Omran HY, El-Hacha R, Nonlinear 3D finite element modeling of RC beams strengthened with prestressed NSM-CFRP strips. Constr Build Mater 2012, 31, 74-85.

[2] El-Hacha R, Wight, RG and Green, MF, Prestressed Fibre- Reinforced Polymer Laminates for Strengthening Structures, Progr in Struct Engrg and Mater J 2000;3, 111-121.

[3] ACI Committee 440. State-of-the-Art Report on Fiber Reinforced Plastic Reinforcement for Concrete Structures (440R-96) (Reapproved 2002), American Concrete Institute, Farmington Hills, 1996, Mich., 68 pp.

[4] Almusallam HT, Elsanadedy MH, Al-Salloum AY, Alsayed HS. Experimental and numerical investigation for the flexural strengthening of RC beams using nearsurface mounted steel or GFRP bars, Constr Build Mater 2013; 40: 145-161.

[5] Soliman S, El Salakawy E, Benmokrane B. Flexural behaviour of concrete beams strengthened with near surface mounted fibre reinforced polymer bars. Can J Civ Eng 2010;37(10):1371–82.

[6] ACI Committee 440. Guide for the design and construction of concrete reinforced with FRP Bars (ACI 440.1R-06), Farmington Hills, Michigan (USA): American Concrete Institute; 2006.

[7] El-Hacha R, Gaafar M. Flexural strengthening of reinforced concrete beams using prestressed near-surface mounted CFRP bars. PCI J Fall 2011:134–51.

[8] El-Hacha R and Soudki K, Prestressed near-surface mounted fibre reinforced polymer reinforcement for concrete structures — a review. Can J Civ Engrg, 2006, 40, 1127-1139.

[9] Gaafar M, El-Hacha R, Strengthening reinforced concrete beams with prestressed near surface mounted FRP strips. Fourth International Conference on FRP Composites in Civil Engineering (CICE2008), 22-24 July 2008, Zurich, Switzerland.

[10] Nordin H, Täljsten B. Concrete beams strengthened with prestressed near surface mounted CFRP. J Compos Constr 2006;10(1):60–8.

[11] Badawi M, Soudki K. Flexural strengthening of RC beams with prestressed NSM CFRP rods – experimental and analytical investigation. Constr Build Mater 2009;23(10):3292–300.

[12] Badawi M. Monotonic and fatigue flexural behavior of RC beams strengthened with prestressed NSM CFRP rods. Ph.D. Thesis, Univ. of Waterloo, Waterloo, Ont., Canada; 2007.

[13] Badawi M, Wahab N, Soudki KA. Evaluation of the transfer length of prestressed near surface mounted CFRP rods in concrete. Constr Build Mater 2011;25(3):1474–9.

[14] Oudah F, El-Hacha R. Fatigue behavior of RC beams strengthened with prestressed NSM CFRP rods. Compos Struct 2012;94(4):1333–42.

[15] Peng H, Zhang J, Cai, CS ang Liu Y, An experimental study on reinforced concrete beams strengthened with prestressed near surface mounted CFRP strips. Engrg Struct,79,222-233.

[16] Casadei, P, Galati N, Boschetto G, Tan KY, Nanni A, and Galecki G. Strengthening of impacted prestressed concrete bridge I-girder using prestressed near surface mounted CFRP bar. Fédération Internationale du Béton (FIB). *In* Proceedings of the 2nd International Congress, Naples, Italy, 5–8 June 2006, Session 10, 10 p.

[17] Choi HT, West JS, and Soudki KA. Effect of partial unbonding on prestressed near-surface-mounted CFRP-strengthened concrete T-beams. *J Compos Constr* 2011, 15(1): 93–102. doi:10.1061/(ASCE)CC. 1943-5614.0000149.

[18] Jung W, Park J, and Park Y. 2007. A study on the flexural behaviour of reinforced concrete beams strengthened with NSM prestressed CFRP reinforcement. *In Proceeding of the 8th International Symposium on Fiber Reinforced Polymer Reinforcement for Reinforced Concrete Structures (FRPRCS-8)*, University of Patras, Patras, Greece, 16–18 July 2007, (CD-Rom) 8 p.

[19] Omran HY, and El-Hacha R. Parametric study of RC girders strengthened in flexure using prestressed NSM CFRP strips. *In Proceedings of the 3rd International Conference on Seismic Retrofitting of Structures (ICSR2010)*, 20–22 October, Tabriz, Iran, 2010, (CD-Rom) 12 p.

[20] Omran HY, and El-Hacha R. Effects of severe environmental exposure on RC beams strengthened with prestressed NSM-CFRP strips. *In Proceedings of the 6th International Conference on FRP Composites in Civil Engineering (CICE 2012)*, Rome, Italy, 13–15 June, 2012, (CD-Rom) 8 p.

[21] Wu Z, Iwashita K, and Sun X. Structural performance of RC beams strengthened with prestressed near-surface-mounted CFRP tendons. *In Proceedings of ACI Special Publication*

SP-245: Case Histories and Use of FRP for Prestressing Applications, Denver, Colorado, USA, 8 November, 2007, Paper SP 245-10, pp. 165–178.

[22] Oudah F, and El-Hacha R. Analytical fatigue prediction model of RC beams strengthened in flexure using prestressed FRP reinforcement. Engrg Struct 2012, 46: 173–183.

[23] Omran HY, and El-Hacha R. 2012. Anchorage system to prestress NSM CFRP strips: Effects of bond and anchor dimensions on the interfacial stress distributions and bond performance. *In Proceedings of the 4th International Symposium on Bond in Concrete (BIC2012)*, Brescia, Italy, 17–20 June, 2012, 8 p.

[24] CEB-FIP. Model code for concrete structures, Comite Euro-International du Beton, Bulletin 213/214; 1990.

[25] Rezazadeh M, Costa I, Barros J. Influence of prestress level on NSM CFRP laminates for the flexural strengthening of RC beams. Compos Struct 2014;116:489–500.

[26] Rezazadeh M, Barros J, Costa I. Analytical approach for the flexural analysis of RC beams strengthened with prestressed CFRP. Compos Part B- Engrg 2015, 73, 16-34.

[27] Michels J, Martinelli E, Czaderski C and Motavalli M. Prestressed CFRP strips with gradient anchorage for structural concrete retrofitting: Experiments and Numerical Modeling. Polymers 2014;6:114-131.

[28] Razaqpur AG, Isgor OB. Methods for calculating deflections of FRP reinforced concrete structures. In: Proceeding of the 3rd international conference on advanced composite materials in bridges and structures, Ottawa, Canada; August 2000. p. 371–378.

[29] Bischoff PH, Deflection calculation of FRP reinforced concrete beams based on modifications to the existing Branson equation, J Compos Constr, 2007, 11(1), 4–14.

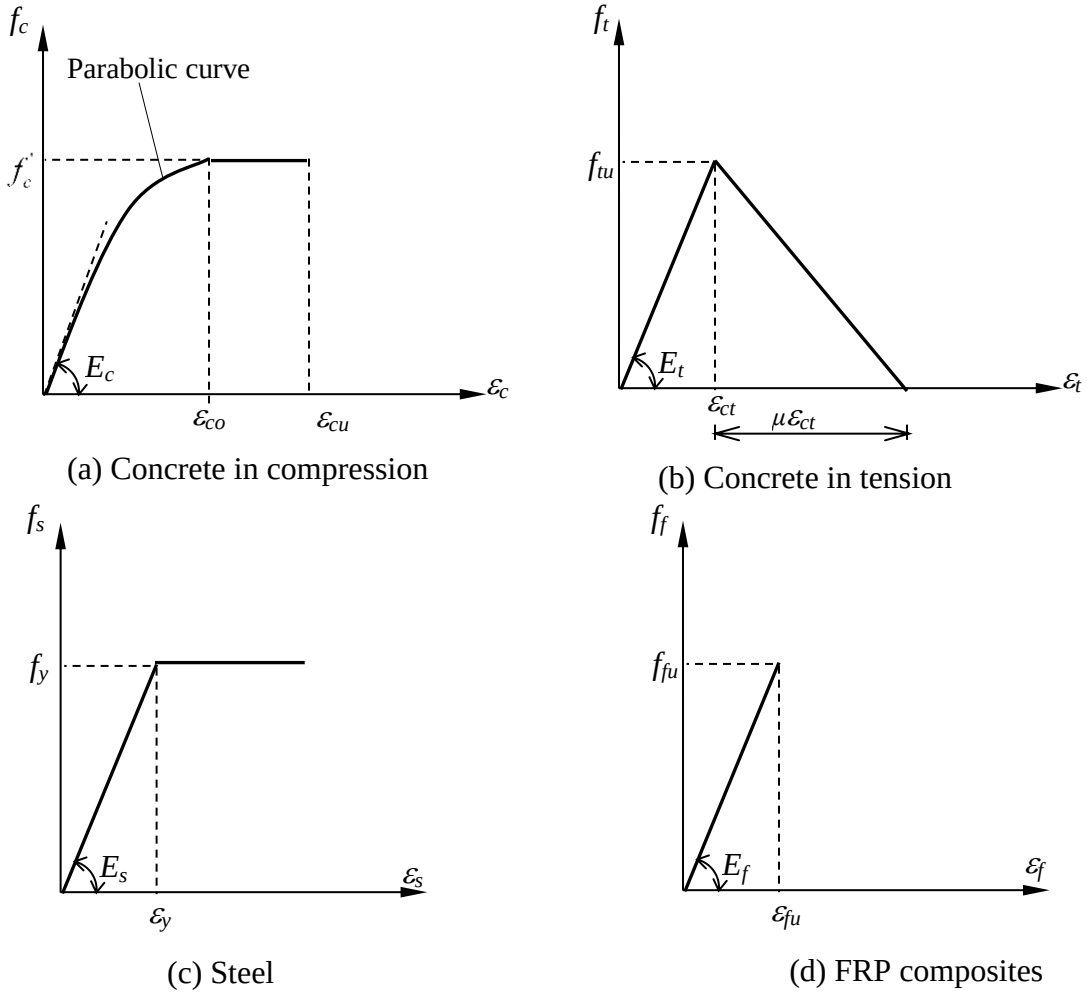

(a) Concrete in compression

(b) Concrete in tension

(c) Steel

(d) FRP composites

Fig. 1 Concrete, steel and FRP stress–strain relationships.

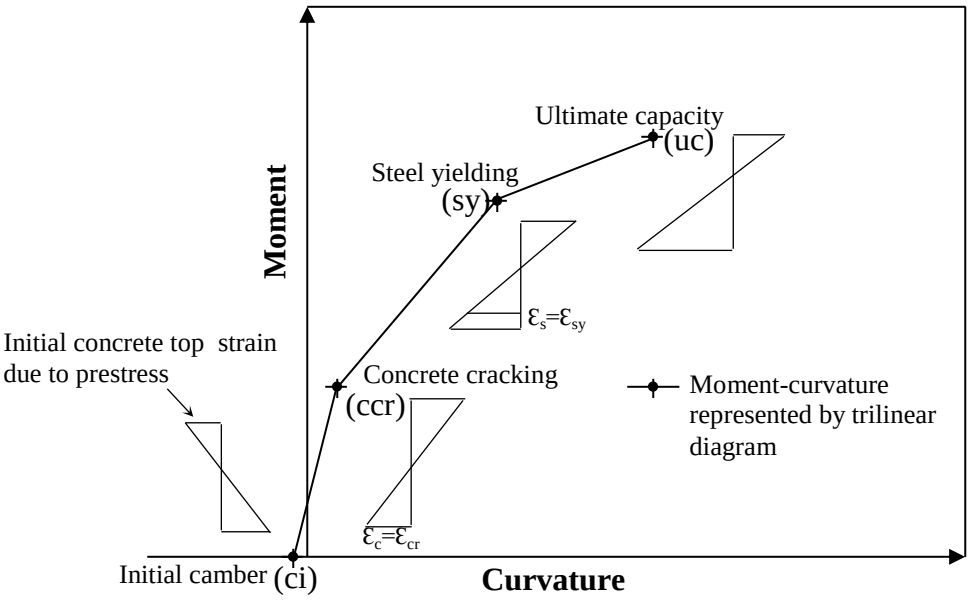

Fig. 2 Critical points of the trilinear moment curvature diagram of reinforced concrete beams strengthened with prestressed strengthened beams.

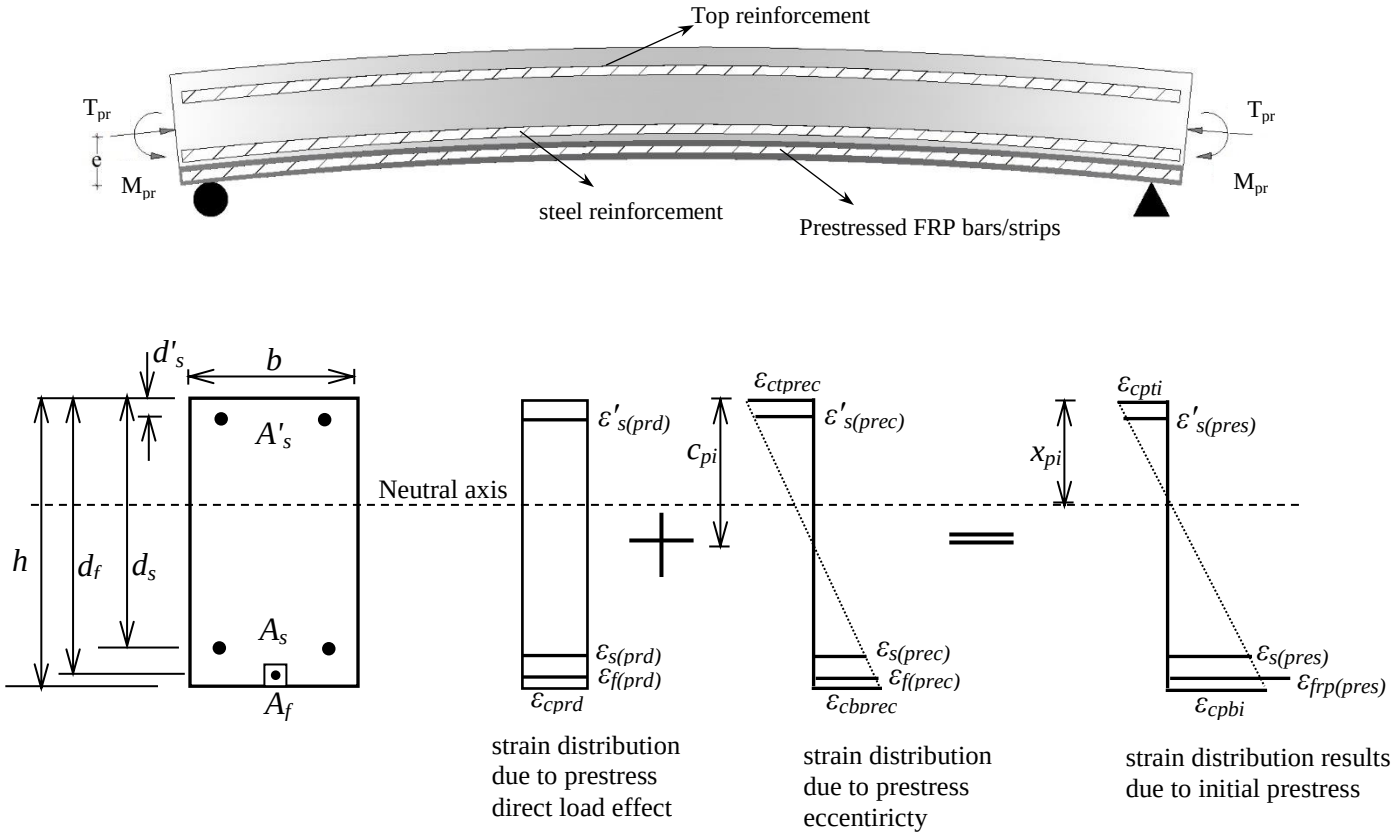

Fig. 3 Strain distributions of reinforced concrete section strengthened with prestressed NSM FRP reinforcement due to initial prestress

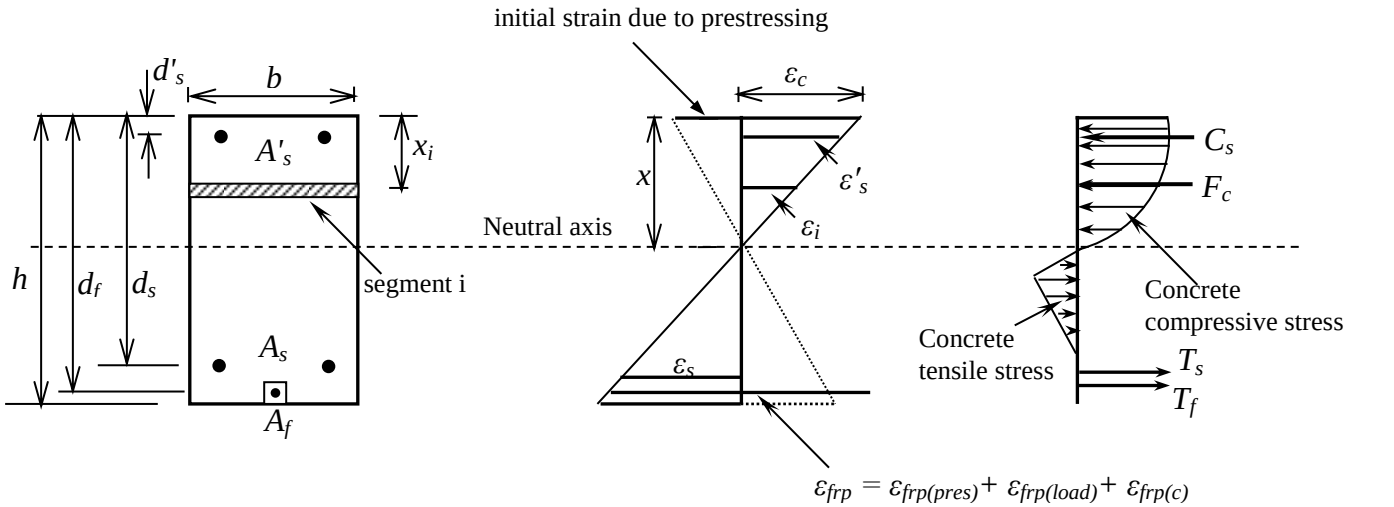

(a) concrete section reinforced with prestressed FRP bars/strips

(b) Strain distribution

(c) Stress distribution and forces

Fig. 4 Strains, stresses and forces of reinforced concrete section strengthened with prestressed NSM FRP reinforcement

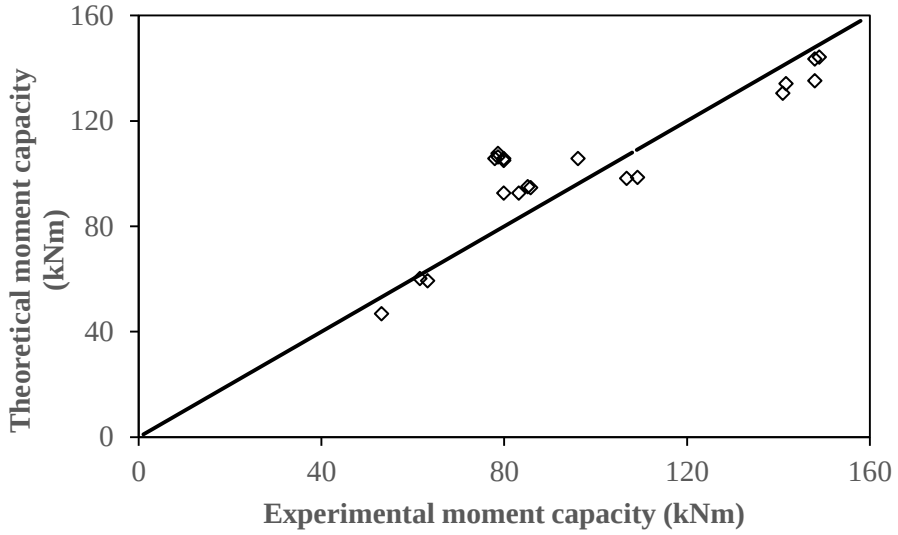

Fig. 5 Experimental versus predicted moment capacities of reinforced concrete beams strengthened with prestressed NSM FRP reinforcement

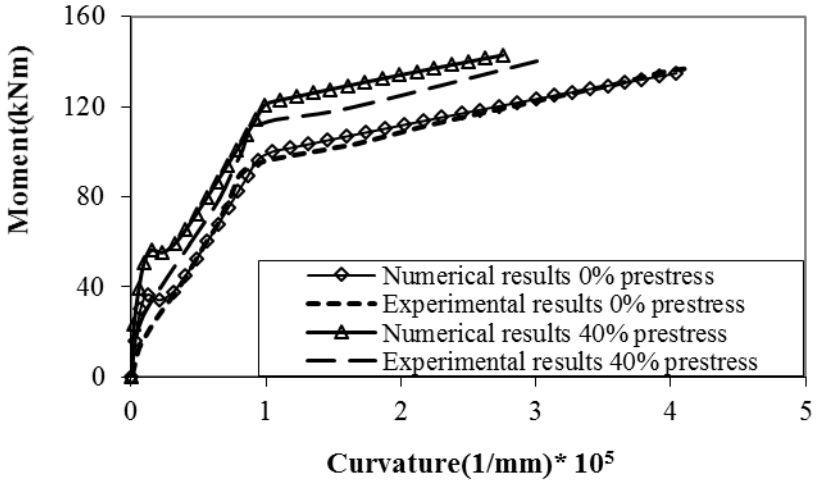

Fig. 6 Comparison of predicted and experimental moment-curvature relationships of reinforced concrete beams strengthened with and without prestressed NSM FRP

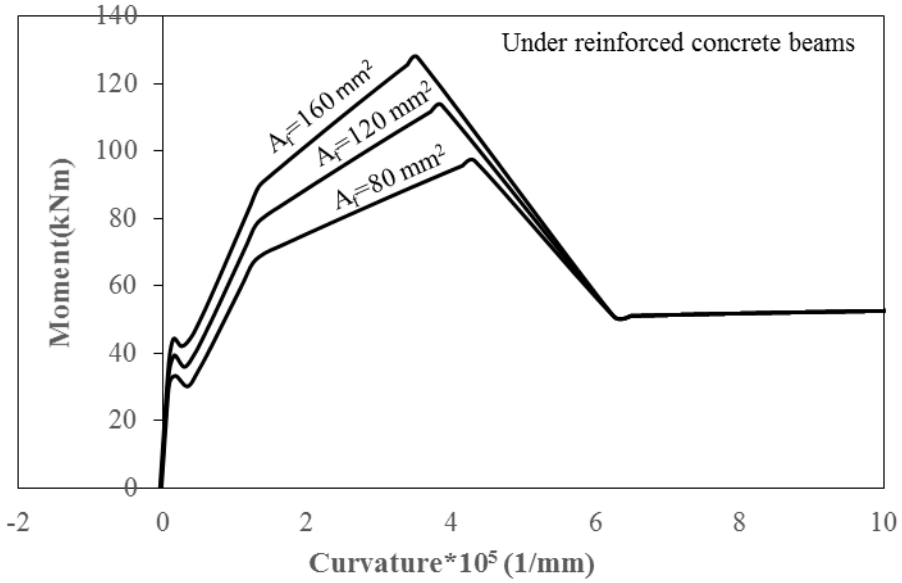

(a) Under reinforced sections

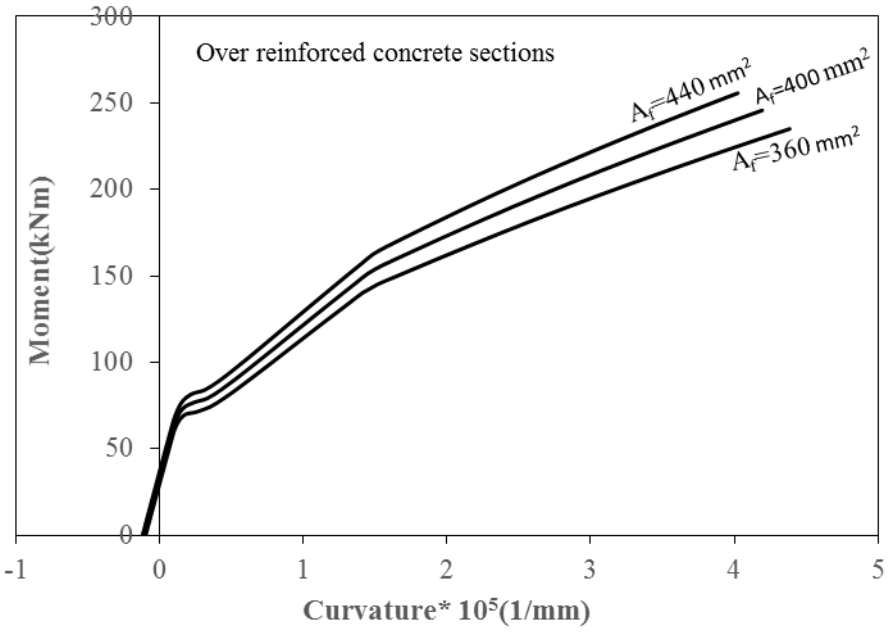

(b) Over reinforced concrete sections

Fig. 7 (a-b) Moment-curvature relationships of under and over reinforced concrete beams strengthened with prestressed FRP bars.

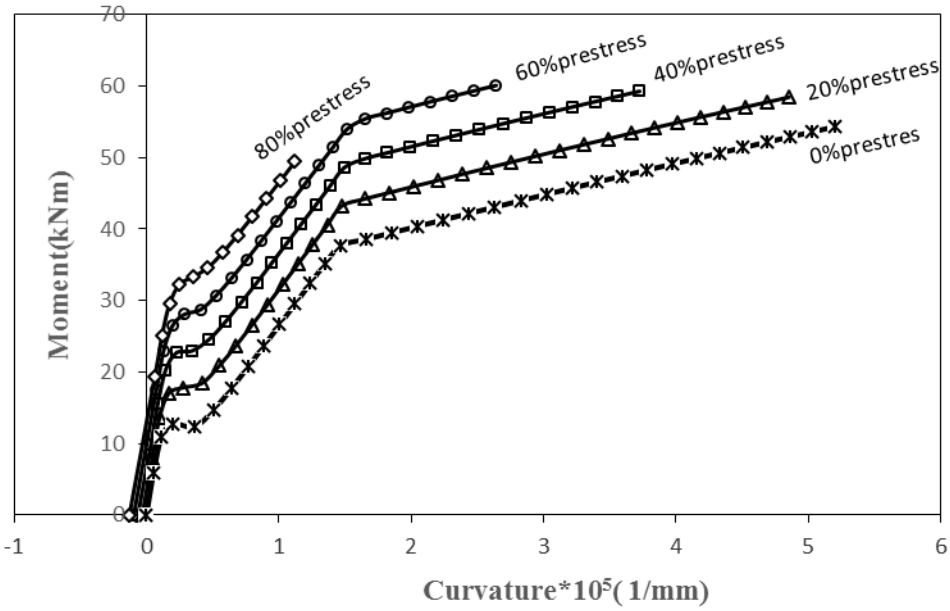

Fig. 8 Effect of prestress level on the flexural behavior of strengthened prestressed beams

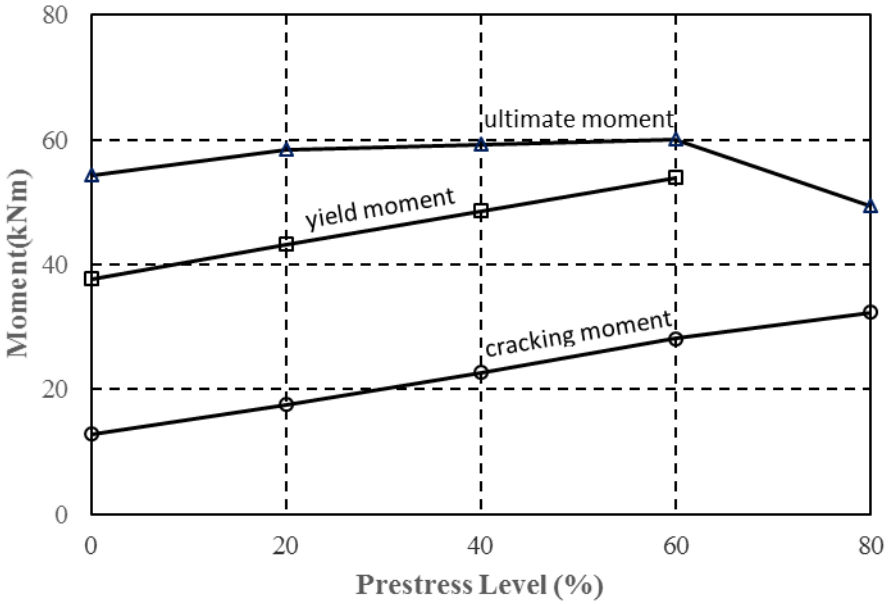

Fig. 9 Effect of increasing the prestressing level on the cracking, yielding, and ultimate moments

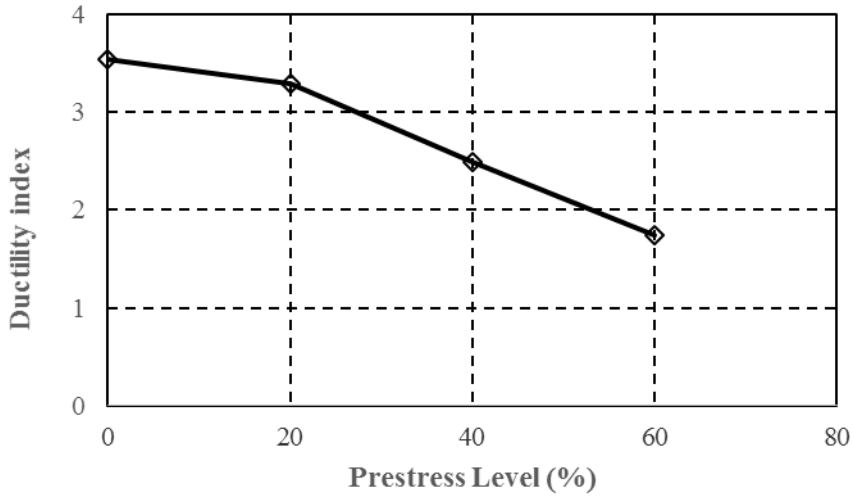

Fig. 10 Effect of increasing the prestressing level on the ductility of concrete beams

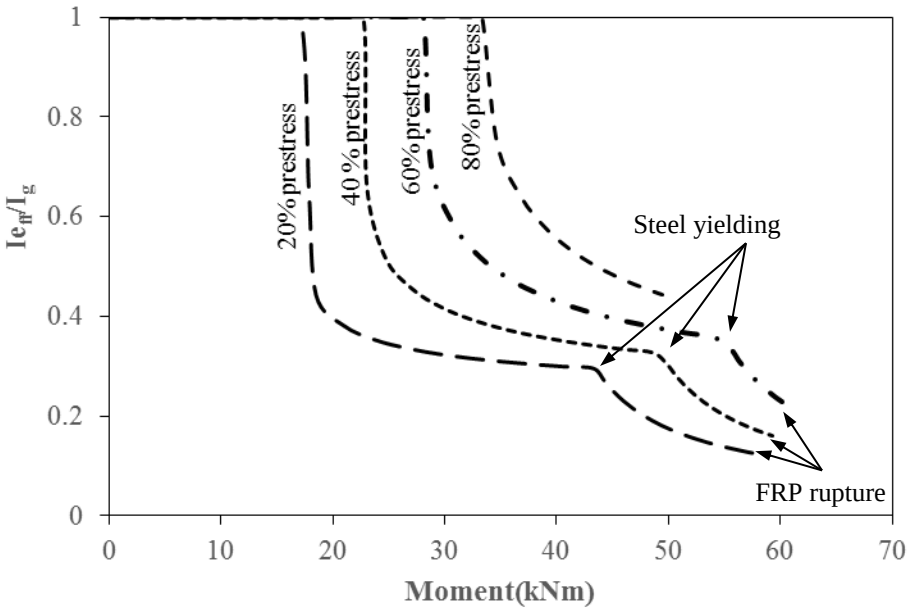

Fig. 11 Effective flexural stiffness variations

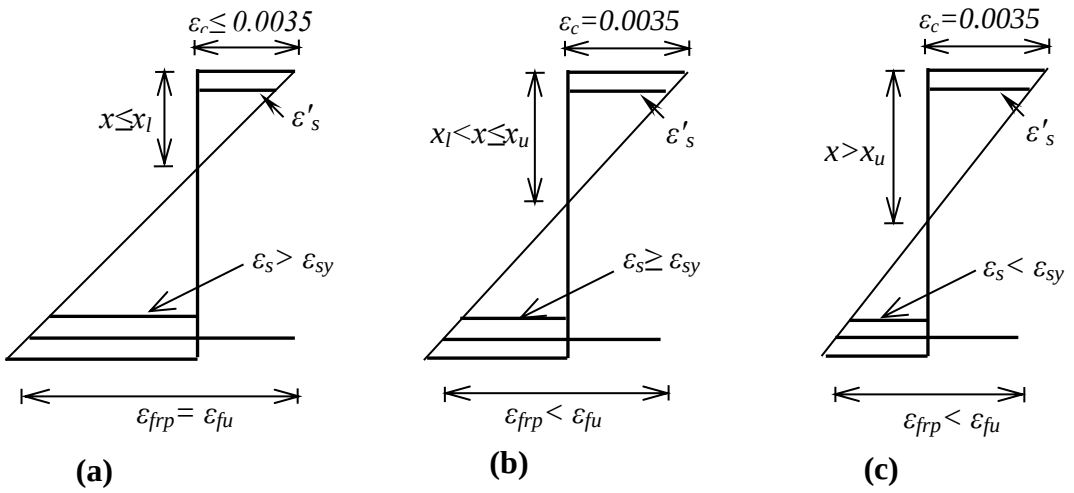

Fig. 12 Strain distributions for different amount of prestressed FRP reinforcement at failure
(a) FRP rupture before concrete crushing ($A_f \leq A_{fl}$) **(b)** Case of ($A_{fl} < A_f \leq A_{fu}$) **(c)** Over-reinforced case ($A_f > A_{fu}$)

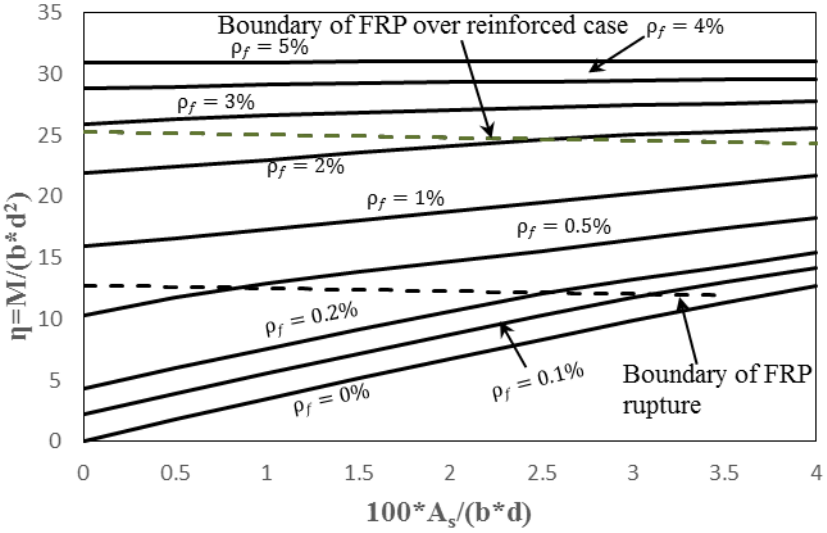

(a) Variation of normalised moment capacity against the area of steel reinforcement

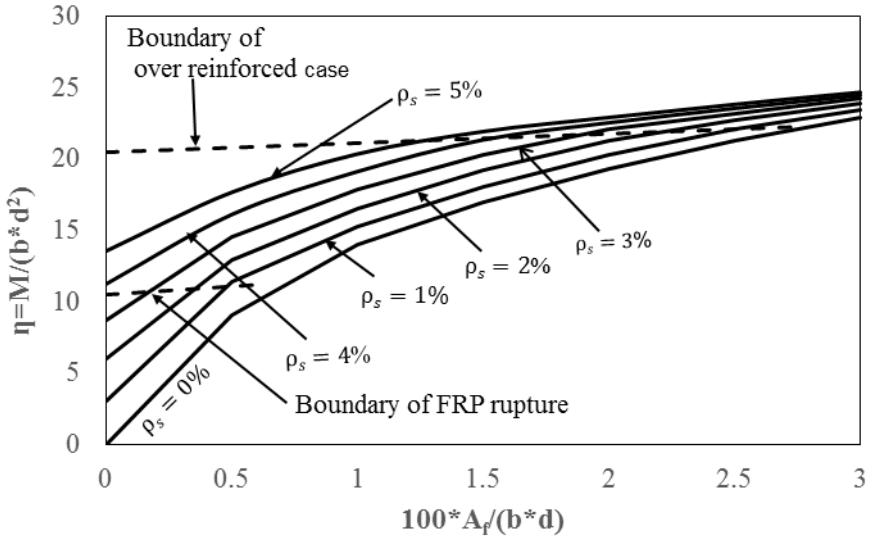

(b) Variation of normalised moment capacity against the area of FRP reinforcement

Fig. 13 (a-b) Effect of steel and FRP reinforcements on the normalised moment capacity

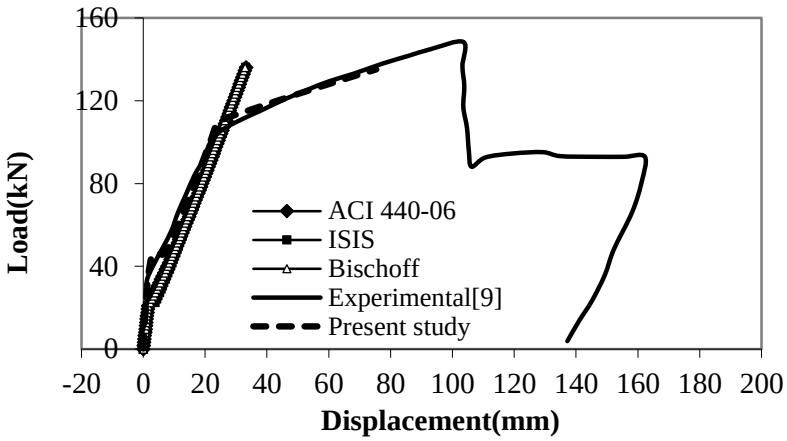

(a) B1-20%

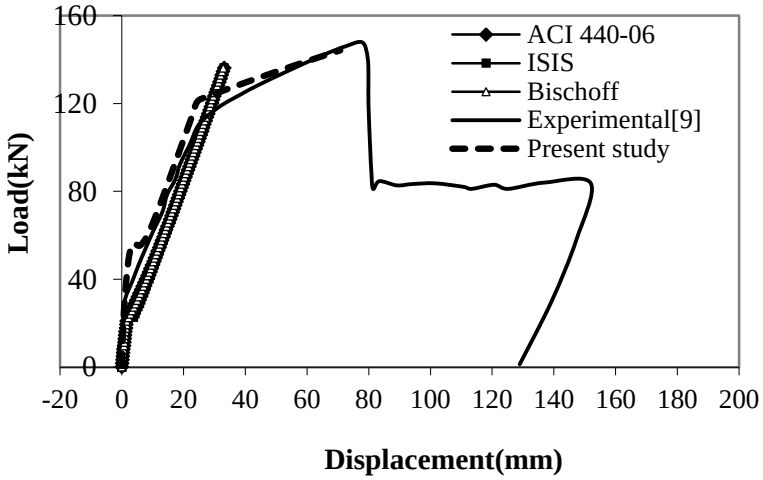

(b) B1-40%

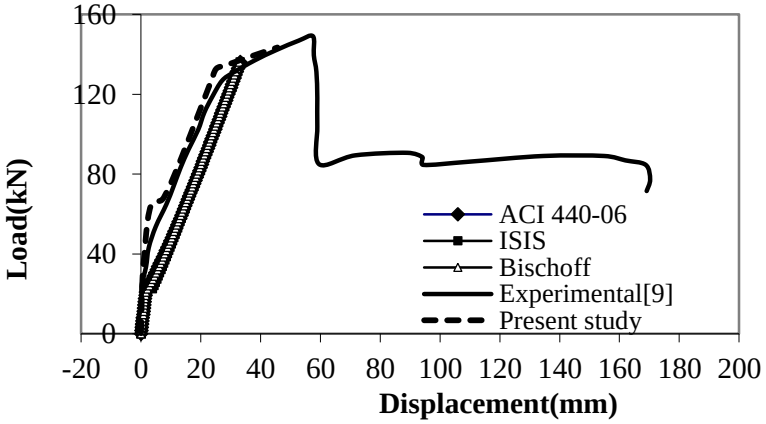

(c) B1-60%

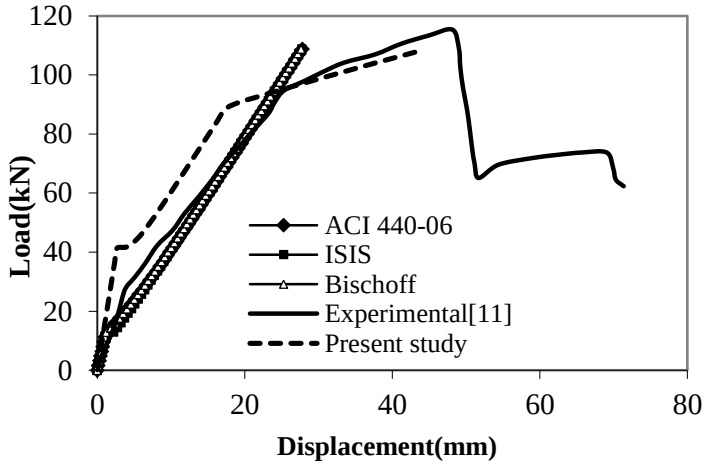

(d) 40% pres.

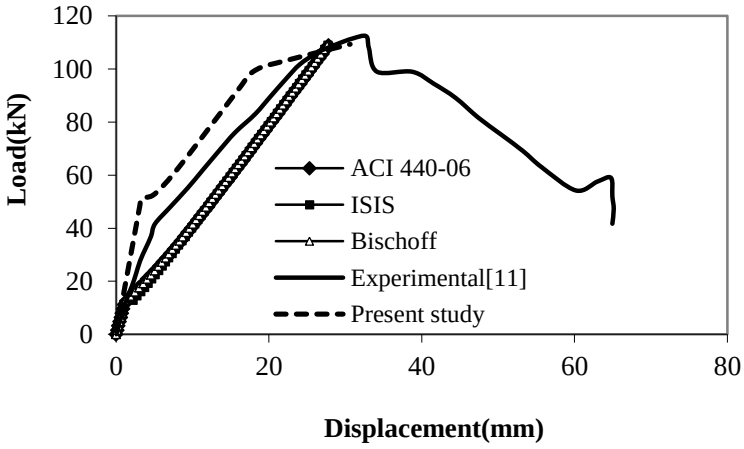

(e) 60% pres.

Fig. 14 (a-e) Comparison between experimental and theoretical deflections of reinforced concrete beams strengthened with prestressed NSM FRP bars tested in the literature

TABLE CAPTIONS

Table 1 Details of concrete beams reinforced with prestressed NSM FRP bars/strips tested in the literature.

Table 2 Comparisons between the theoretical and experimental flexural moment capacities of concrete beams reinforced with prestressed NSM FRP bars/strips tested in the literature.

Table 1 Details of concrete beams reinforced with prestressed NSM FRP bars/strips tested in the literature.

Reference	Beam notation	Width (mm)	Overall depth (mm)	Span (mm)	$f_c^{'}$ (MPa)	A_f (mm^2)	A_s (mm^2)	E_f (kN/mm^2)	*Prestress* (N/mm^2)	*Type of FRP*
[7]	B2-20%	200	400	5000	40.7	65	600	130	421	CFRP rods
	B2-40%	200	400	5000	40	65	600	130	807	CFRP rods
[9]	B1-20%	200	400	5000	40	64	600	145	522	CFRP strips
	B1-40%	200	400	5000	40	64	600	145	1044	CFRP strips
	B1-60%	200	400	5000	40	64	600	145	1566	CFRP strips
[10]	BPM1	200	300	3600	63	100	402	250	320	CFRP rods
	BPM2	200	300	3600	62	100	402	250	320	CFRP rods
	BPM3	200	300	3600	65	100	402	250	540	CFRP rods
	BPM4	200	300	3600	66	100	402	250	380	CFRP rods
	BPS1	200	300	3600	68	100	402	160	290	CFRP rods
	BPS2	200	300	3600	68	100	402	160	300	CFRP rods
	BPS3	200	300	3600	66	100	402	160	330	CFRP rods
	BPS4	200	300	3600	64	100	402	160	350	CFRP rods
	BPS5	200	300	3600	67	100	402	160	560	CFRP rods
	BPS6	200	300	3600	67	100	402	160	560	CFRP rods
[11]	40% pres	152	254	3300	47.9	70.85	353.25	136	788	CFRP bar
	60% pres	152	254	3300	47.9	70.85	353.25	136	1182	CFRP bar
[15]	PRS2N20-	200	300	3300	51.68	64	402	131	1000	CFRP strips
	PRS2N20-AN	200	300	3300	50.58	64	401	131	1000	CFRP strips
[18]	ROD-PRE-20	200	300	3400	31.3	63.6	213	121	375	CFRP strips

Note: E_f is the modulus of elasticity of prestressed FRP longitudinal bars/strips, A_f and A_s are FRP and steel reinforcement areas and $f_c^{'}$ is the cylinder compressive strength of concrete. If concrete cylinder compressive strength $f_c^{'}$ is not measured in experimental investigation, it is assumed that $f_c^{'} = 0.85 f_{cu}$, where f_{cu} is the concrete cube compressive strength.

Table 2 Comparisons between the theoretical and experimental flexural moment capacities of concrete beams reinforced with prestressed NSM FRP bars/strips tested in the literature.

Reference	Beam notation	M_{exp} (kN)	M_{pred} (kN)	M_{pred}/M_{exp}	Experimental mode of failure
[7]	B2-20%	141	130.5	0.93	SY-FRPR
	B2-40%	141.7	134.12	0.95	SY-FRPR
[9]	B1-20%	148	135.28	0.91	SY-FRPR
	B1-40%	149	144.37	0.97	SY-FRPR
	B1-60%	148	143.71	0.97	SY-FRPR
[10]	BPM1	83.2	92.74	1.11	SY-FRPR
	BPM2	85.8	94.77	1.1	SY-FRPR
	BPM3	85.15	95.26	1.12	SY-FRPR
	BPM4	79.95	92.72	1.16	SY-FRPR
	BPS1	78.65	106.17	1.35(1.12)**	SY-FRPR
	BPS2	78.65	106.36	1.35(1.12)**	SY-FRPR
	BPS3	78	105.8	1.35(1.13)**	SY-FRPR
	BPS4	79.95	105	1.31(1.07)**	SY-FRPR
	BPS5	79.9	105.86	1.32(1.08)**	SY-FRPR
	BPS6	96.2	105.86	1.1(0.9)**	SY-CC*
[11]	40% pres	63.25	59.45	0.94	SY-FRPR
	60% pres	61.6	60.36	0.98	SY-FRPR
[15]	PRS2N20-BL330	109.2	98.73	0.9	SY-FRPR
	PRS2N20-AN	106.8	98.38	0.92	SY-FRPR
[18]	ROD-PRE-20	53.18	46.83	0.87	SY-FRPR
			Average	**1.08(1.01)****	
			Standard deviation (%)	**17.2% (9.7%)****	
			Coefficient of variation (%)	**15.93% (8.82%)****	

Note: M_{exp} and M_{the} are the experimental and theoretical moment capacities of prestressed FRP strengthened sections. Experimental failure modes: SY-CC refers to steel yielding followed by concrete crushing and SY-FRPR indicates steel yielding followed by FRP rupture modes of failure.
*Indicates disagreement between predicted and experimentally observed flexural failure modes.
** Values in brackets are the ratio between predicted and experimental moment capacities when the tensile strength of CFRP bars in beams BPS1 to BPS5 is assumed as that for beams BM1 to BM4 of the same investigation.